

# Neural-network quantum state study of the long-range antiferromagnetic Ising chain

Jicheol Kim,<sup>1</sup> Dongkyu Kim,<sup>1,2</sup> and Dong-Hee Kim<sup>1,\*</sup>

<sup>1</sup>*Department of Physics and Photon Science, Gwangju Institute of Science and Technology, Gwangju 61005, Korea*

<sup>2</sup>*Kakao Corporation, Pangyo, Gyeonggi 13529, Korea*

We investigate quantum phase transitions in the transverse field Ising chain with algebraically decaying long-range antiferromagnetic interactions by using the variational Monte Carlo method with the restricted Boltzmann machine being employed as a trial wave function ansatz. In the finite-size scaling analysis with the order parameter and the second Rényi entropy, we find that the central charge deviates from 1/2 at a small decay exponent  $\alpha_{LR}$  in contrast to the critical exponents staying very close to the short-range (SR) Ising values regardless of  $\alpha_{LR}$  examined, supporting the previously proposed scenario of conformal invariance breakdown. To identify the threshold of the Ising universality and the conformal symmetry, we perform two additional tests for the universal Binder ratio and the conformal field theory (CFT) description of the correlation function. It turns out that both indicate a noticeable deviation from the SR Ising class at  $\alpha_{LR} < 2$ . However, a closer look at the scaled correlation function for  $\alpha_{LR} \geq 2$  shows a gradual change from the asymptotic line of the CFT verified at  $\alpha_{LR} = 3$ , providing a rough estimate of the threshold being in the range of  $2 \lesssim \alpha_{LR} < 3$ .

## I. INTRODUCTION

Artificial neural networks and machine learning have been influencing the paradigm of physics research with a growing number of applications on various subjects, including phase transitions and critical phenomena in classical and quantum many-body systems [1–4]. In particular, the representation of a quantum wave function by a neural network [5] provides an alternative numerical platform combined with the variational Monte Carlo (VMC) method to find the ground state of a many-body Hamiltonian. The neural-network quantum state (NQS) has extended its area of applications to the Fermi and Bose Hubbard models [6, 7], real-time dynamics [5, 8], open quantum systems [9–12], quantum state tomography [13, 14], frustrated systems [15–21], and *ab initio* simulations of molecules [22–24]. The NQS ansatz offers the high expressive capacity often measured in terms of entanglement scaling [25–29], proposing a complementary tool to conventional numerical methods for studying quantum criticality.

In this paper, we investigate quantum phase transitions in the transverse field Ising chain (TFIC) with algebraically decaying long-range (LR) antiferromagnetic (AF) interactions by employing the NQS ansatz for the VMC calculations. LR-interacting quantum systems have attracted growing attention, both theoretical and experimental [30]. The trapped-ion quantum simulation [31] realized the TFIC Hamiltonian with an LR interaction that maps to the form of  $1/r^{\alpha_{LR}}$  with a tunable exponent  $\alpha_{LR}$ , providing a controllable experimental platform to study quantum phase transitions at and out of equilibrium [32–34]. The nearest-neighbor-interacting short-range (SR) TFIC is a textbook example of quantum critical behavior in one dimension (1D) that belongs to the universality class of the classical two-dimensional (2D) Ising model [35]. However, such quantum-classical correspondence to the universality of critical phenomena becomes nontrivial in presence of LR interactions. A central question of how criticality depends on  $\alpha_{LR}$  is still an active subject of various numerical and analytical

studies [30, 36–60].

We revisit this question in the AF side of the LR interactions for TFIC where the breakdown of the Ising class in the critical ground state seems to be very different from what is established in the ferromagnetic (FM) counterpart [47–51, 55–57]. Because an exact solution is not available, constructing the picture of how its criticality deviates from the Ising class as  $\alpha_{LR}$  decreases relies primarily on the collection of numerical observations. Despite various numerical studies characterizing the quantum phase transition in AF-LR-TFIC [52–58], the picture remains incomplete in some parts, demanding more numerical evidence for clarification. Using the restricted Boltzmann machine (RBM) for the NQS ansatz [5], we consider the moments of staggered magnetization including the order parameter and the Binder ratio, the two-point correlation function, and the entanglement entropy to examine the present picture and find clearer signatures of the breakdown of the SR Ising class and the conformal invariance along the critical line.

We begin with brief reviews of previous results on the characterization of the criticality. The first study of AF-LR-TFIC [52] using the time-dependent variational principle (TDVP) found a phase transition for all  $\alpha_{LR} > 0$ , where it turned out that the critical exponent of the correlation function decreases from the SR Ising value for  $\alpha_{LR} \lesssim 2$ . A significant increase in the central charge from the Ising value 1/2 was observed at  $\alpha_{LR} \lesssim 1$  in the TDVP [52] and density matrix renormalization group (DMRG) [53] calculations, based on which the breakdown of conformal invariance was proposed [53]. While here we focus on the critical ground state, a violation of the area law for the entanglement entropy was observed in the offcritical area [52, 53, 58], and it was shown that the area law of the noncritical ground state holds for  $\alpha_{LR} > 2$  [61].

On the other hand, contrasting evidence was found in the other DMRG calculations [54, 55], where the estimates of the critical exponents  $\nu \simeq 1$  and  $\beta \simeq 1/8$  and the dynamic exponent  $z \simeq 1$  were in agreement with the SR Ising values for all examined  $\alpha_{LR}$  between 0.4 and 3. However, these DMRG estimates of the critical exponents have not been fully verified in different approaches. Linked cluster expansion calculations [56] reported  $z\nu = 1.7(5)$  for  $\alpha_{LR} = 2$  while  $z\nu \approx 1$  for  $\alpha_{LR} = 9/4$ . Previous quantum Monte Carlo (QMC) calculations with

\* dongheekim@gist.ac.kr

stochastic series expansion [57] provided lower values of  $\nu$  and  $\beta$  in its examined range of  $\alpha_{\text{LR}} \geq 2$ . Nonetheless, these TDVP and DMRG results altogether suggest an interesting possibility that some of the exponents are still very close to the SR Ising values even for such a small  $\alpha_{\text{LR}}$  despite the deviation in the central charge.

This scenario was proposed in the study of the Kitaev chain with LR pairing [59, 60] which becomes equivalent to the Ising chain only in the SR limit. Along the critical line of a positive chemical potential, the conformal invariance is broken for  $\alpha_{\text{LR}} < 2$  while the Ising exponent  $\beta$  is unchanged in the test of a quantity that corresponds to the Ising order parameter in the SR limit. Although there is no rigorous mapping between the Kitaev chain and the Ising model at a finite  $\alpha_{\text{LR}}$ , the empirical similarity between the scenario of conformal symmetry breakdown in the Kitaev chain and the previous TDVP and DMRG observations in AF-LR-TFIM motivates us to revisit the phase transition in this LR Ising system to examine the breakdown of the Ising universality and the conformal invariance in different numerical approaches.

Our VMC+RBM calculations investigate this scenario. In the finite-size scaling (FSS) analysis of the order parameter extracted from the ground-state RBM wave function for  $0.5 \leq \alpha_{\text{LR}} \leq 3$ , we find that our estimates of the critical exponents  $\nu$  and  $\beta$  are indeed very close to the SR Ising values for all the values of  $\alpha_{\text{LR}}$  examined, which is in agreement with the previous DMRG results [54, 55]. The susceptibility exponent  $\gamma$  is also close to the SR Ising value, but with a much larger error bar. On the other hand, we find a deviation in the correlation function exponent and the central charge from the SR Ising class at a small  $\alpha_{\text{LR}}$ . In particular, our estimate of the central charge extracted from the second Rényi entropy under the periodic boundary conditions (PBC) is smaller than  $1/2$  at  $\alpha_{\text{LR}} \lesssim 1$ . This decrease contrasts with the increase indicated by the previous measurement with the von Neumann entropy in an open chain [52, 53], which is also possibly related to the breakdown of the conformal invariance.

To identify the threshold value of  $\alpha_{\text{LR}}$  below which the SR Ising universality and the conformal invariance are broken, we additionally examine the critical Binder ratio [40] and the CFT description of the universal form of the correlation function [62]. Both tests indicate a clear signal of such breakdown at  $\alpha_{\text{LR}} < 2$ , which strengthens the similar evidence found in the measurement of the critical exponent  $\eta$  of the correlation function. On the other hand, a closer look at the scaled correlation function [62] indicated a gradual change in the asymptotic line predicted by the CFT as  $\alpha_{\text{LR}}$  decreases away from 3 where the prediction of the CFT in the SR limit is well verified. These observations suggest a rough estimate of the threshold being in the range of  $2 \leq \alpha_{\text{LR}} < 3$ .

This paper is organized as follows. The AF-LR-TFIC model Hamiltonian and the numerical details of the VMC+RBM calculations are described in Sec. II. The main results are given in Sec. III. In the subsections, the FSS analysis for the estimate of the critical exponents and the extraction of the central charge from the second Rényi entropy are given, and then the tests of the critical Binder ratio and the CFT prediction of the correlation function are presented. The summary and conclusions

are given in Sec. IV.

## II. MODEL AND VMC+RBM CALCULATIONS

We consider the AF-LR-TFIC Hamiltonian [52] given as

$$\hat{H} = \sin \theta \sum_{i < j} J_{ij} \hat{\sigma}_i^x \hat{\sigma}_j^x + \cos \theta \sum_i \hat{\sigma}_i^z, \quad (1)$$

where  $\theta$  is in the range of  $0 < \theta < \pi/2$  for the AF coupling, and the site indices  $i$  and  $j$  run from 1 to  $L$  in the chain of length  $L$ . We impose PBC as the boundary conditions that are necessary for the test of the CFT description of the correlation function constructed in a cylindrical space-time geometry. In the implementation of the algebraically decaying LR interaction under PBC, we choose to write  $J_{ij}$  with a range cutoff that increases with the system size  $L$  by adopting the formulation used in the LR-Kitaev chain [59, 60] as

$$J_{ij} = \begin{cases} |i - j|^{-\alpha_{\text{LR}}} & \text{for } |i - j| < L/2, \\ (L - |i - j|)^{-\alpha_{\text{LR}}} & \text{for } |i - j| > L/2. \end{cases} \quad (2)$$

We choose RBM as an ansatz for the trial wave function in the VMC simulations to find a ground state [5]. A general state can be expressed as  $|\Psi\rangle = \sum_{\mathbf{s}} \Psi(\mathbf{s}; \mathcal{W}) |\mathbf{s}\rangle$  for the input  $\mathbf{s} = (s_1, s_2, \dots, s_L)$  of RBM, where  $s_i$  indicates  $\sigma_i^x$  in the  $\hat{\sigma}^x$ -basis of the given Hamiltonian. We impose the translation symmetry under PBC to reduce the number of variational parameters. Following the procedures of Ref. [5], after integrating out the Ising spins in the hidden layer, one can find the expression of the RBM wave function,

$$\Psi(\mathbf{s}; \mathcal{W}) = e^{a \sum_{j=1}^L s_j} \prod_{m=1}^L \prod_{i=1}^{n_h} \cosh \left[ b_i + \sum_{j=1}^L W_{ij} T_m(s_j) \right], \quad (3)$$

where the translation operator  $T$  is defined as  $T_m(s_j) = s_{j+m}$  with periodicity  $s_{j+L} = s_j$ , and  $n_h$  is the number of filters given for the symmetry. On a diagram of RBM, one may illustrate the hidden layer with  $N_h = L n_h$  neurons with  $L$ -fold degeneracy of the neural variables to enforce the translational invariance. In Eq. (3), there are  $(1 + n_h + L n_h)$  RBM parameters of  $\mathcal{W} \equiv \{\mathbf{a}, \mathbf{b}, \mathbf{W}\}$  to be optimized using the VMC method. We adopt complex-valued parameters as suggested in Ref. [5] for better convergence, although the TFIC Hamiltonian is stoquastic [63]. We initialize the RBM by setting  $a = 0$  and assigning Gaussian random numbers with zero mean and variance of  $1/(L n_h)$  to  $\mathbf{b}$  and  $\mathbf{W}$ .

In VMC calculations, we optimize the RBM parameters using the stochastic reconfiguration (SR) method to construct the natural gradient [64–66]. The SR method can be described as the imaginary time evolution of a quantum state, providing a new state projected in the space of  $\{|\Psi\rangle, \partial_1 |\Psi\rangle, \partial_2 |\Psi\rangle, \dots\}$ , where  $\partial_i |\Psi\rangle \equiv \frac{\partial |\Psi\rangle}{\partial \mathcal{W}_i}$ . These procedures propose an update of the variational parameter as  $\mathcal{W}_i^{\text{new}} = \mathcal{W}_i^{\text{old}} + \gamma_{\text{SR}} \delta \mathcal{W}_i$ , where  $\delta \mathcal{W}_i$  is determined by solving the linear equation  $\mathbf{S} \delta \mathcal{W} = -\mathbf{f}$ . The essential numerical procedures are to evaluate the overlap

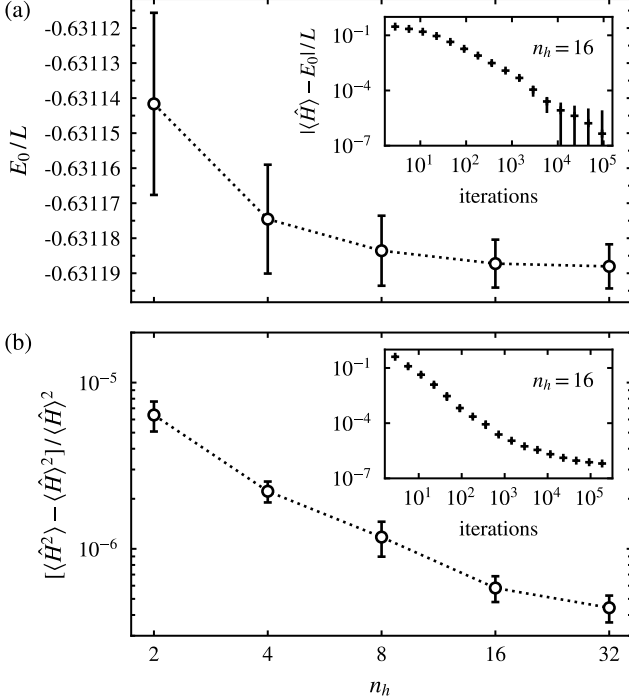


FIG. 1. Convergence test of the RBM wave function in the VMC search for the ground state. The example shown here is for the system of the size  $L = 64$  at  $\alpha_{LR} = 0.5$ . The estimates of (a) energy density  $E_0/L$  and (b) relative variance  $(\langle \hat{H}^2 \rangle - \langle \hat{H} \rangle^2)/\langle \hat{H} \rangle^2$  are measured after  $2 \times 10^5$  iterations and plotted as a function of  $n_h$ . The insets show the same quantities for a fixed number of filters  $n_h = 16$  monitored during the SR iterations of the parameter updates. The data points in the insets represent the averages measured in the logarithmic bins of iteration numbers. The error bars are measured from ten independent RBM wave function samples.

matrix  $\mathbf{S}$  and the force vector  $\mathbf{f}$ ,

$$S_{ij} = \langle \Delta_i^* \Delta_j \rangle_{mc} - \langle \Delta_i^* \rangle_{mc} \langle \Delta_j \rangle_{mc}, \quad (4)$$

$$f_i = \langle \Delta_i^* E_{loc} \rangle_{mc} - \langle \Delta_i^* \rangle_{mc} \langle E_{loc} \rangle_{mc}, \quad (5)$$

where the derivative  $\Delta_i$  and the local energy  $E_{loc}$  are

$$\Delta_i \equiv \frac{\partial_i \Psi(\mathbf{s}; \mathcal{W})}{\Psi(\mathbf{s}; \mathcal{W})} \quad \text{and} \quad E_{loc} \equiv \sum_{\mathbf{s}'} \langle \mathbf{s} | \hat{H} | \mathbf{s}' \rangle \frac{\Psi(\mathbf{s}'; \mathcal{W})}{\Psi(\mathbf{s}; \mathcal{W})}. \quad (6)$$

The expression  $\langle A \rangle_{mc} \equiv \sum_{\mathbf{s}} P(\mathbf{s}) A(\mathbf{s})$  indicates the Monte Carlo measurement of  $A(\mathbf{s})$  with probability  $P(\mathbf{s}) \propto |\Psi(\mathbf{s}; \mathcal{W})|^2$ . We use the conjugate gradient algorithm with the Jacobi preconditioner to solve the linear equation without explicitly storing the  $S$  matrix following the strategy to reduce computational costs proposed in Ref. [66]. For numerical stability, we use the regularization scheme introduced in Ref. [5], where at the  $p$ -th SR iteration,  $S_{ij}$  is replaced by  $S_{ij}(1 + \lambda_p \delta_{ij})$  with  $\lambda_p = \max(\lambda_0 b^p, \lambda_{\min})$ . We use the parameters  $\lambda_0 = 100$ ,  $b = 0.9$ , and  $\lambda_{\min} = 0.01$ . The learning rate  $\gamma_{SR}$  is initially set to 0.1 and increased by 0.1 at every 10000 SR iterations until it becomes unity.

We monitor the convergence of  $|\Psi\rangle$  to the ground state by

evaluating  $\langle \hat{H} \rangle$  and the relative variance defined as

$$\tilde{\sigma}_E \equiv \frac{\langle \hat{H}^2 \rangle - \langle \hat{H} \rangle^2}{\langle \hat{H} \rangle^2}. \quad (7)$$

The relative variance  $\tilde{\sigma}_E$  decreases to zero when  $|\Psi\rangle$  becomes an exact eigenstate. However, in practice, it does not decrease below a certain value in VMC simulations. Probable systematic causes apart from the issues of a global optimization problem may include the limited expressive power of a finite-size neural network despite the universal approximation theorem and unavoidable stochastic fluctuations in the Monte Carlo measurements.

Figure 1 presents an example of the convergence test performed at the critical point in the system of size  $L = 64$  at the LR exponent  $\alpha_{LR} = 0.5$ . Convergence tends to worsen as  $\alpha_{LR}$  decreases in this LR-AF system. At the critical point, convergence typically takes about an order of  $10^5$  iterations to make the energy and variance saturated within the scale of their fluctuations over the iterations. We find that the accuracy level indicated by  $\tilde{\sigma}_E$  after saturation depends essentially on the number of filters  $n_h$ . In our search for the ground state, we set the convergence criterion as  $\tilde{\sigma}_E < 10^{-6}$ , which, for example, is achieved for  $n_h > 8$  in Fig. 1. In our convergence tests,  $n_h = 16$  suffices for system sizes up to  $L = 128$  at the values of  $\alpha_{LR}$  that we examine in this study.

### III. RESULTS AND DISCUSSIONS

Using the RBM wave function obtained for the ground state in the VMC optimizations, we compute the statistics of staggered magnetization including the AF order parameter, the two-point correlation function, and the second Rényi entanglement entropy. Observables are measured with  $4 \times 10^8$  configurations of  $\mathbf{s}$  obtained using the Metropolis sampling algorithm for the probability distribution  $P(\mathbf{s}) \propto |\Psi(\mathbf{s}; \mathcal{W}_{\text{opt}})|^2$ , where  $\mathcal{W}_{\text{opt}}$  is the optimized parameter set. The measurement error for a fixed RBM turns out to be much smaller than the fluctuations over the RBM wave function samples obtained in independent optimizations. The error bars are estimated with ten RBM samples. We specify an error bar if it is larger than a marker size in the plots.

In this section, we first provide our estimates of the critical exponents and the central charge for verification of the previous TDVP and DMRG results. Then, we proceed to present our additional test results with the critical Binder ratio and the universal form of the correlation function to identify the threshold of the breakdown of the SR Ising universality and the conformal symmetry.

#### A. Order parameter and critical exponents

The emergence of the AF order can be detected by measuring the staggered magnetization at the level of RBM. In the AF phase, the operator  $\hat{M}_s = \sum_i (-1)^i \hat{\sigma}_i^x$  in each parity sector of the  $\mathbb{Z}_2$  symmetry indicates a finite positive or negative expectation value. Although Monte Carlo sampling does

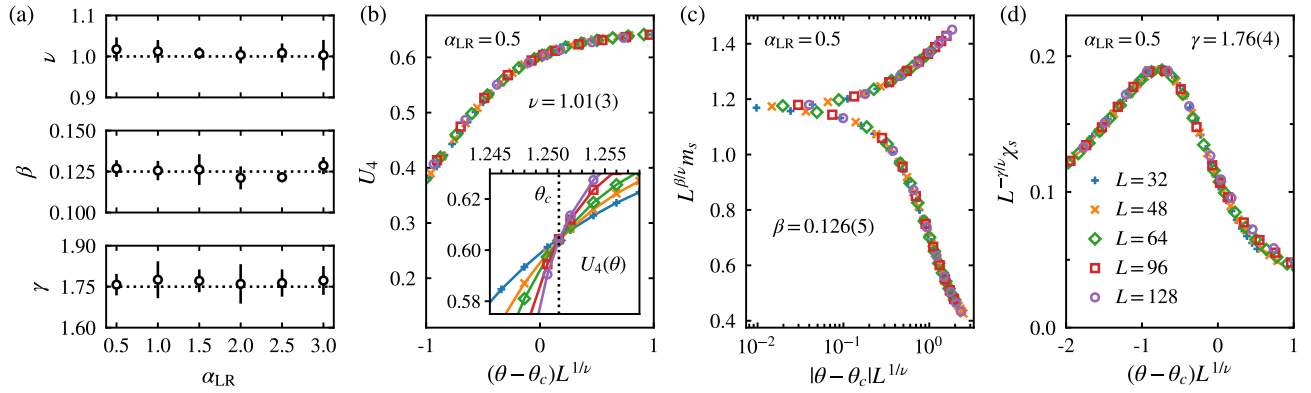


FIG. 2. FSS analysis for critical exponents. (a) The estimates of the critical exponents  $\nu$ ,  $\beta$ ,  $\gamma$  are plotted in the range of  $\alpha_{\text{LR}}$  between 0.5 and 3. The dotted lines given for comparison indicate the SR Ising values. The FSS analysis of scaling curve collapse to measure critical exponents is demonstrated for (b) the fourth-order Binder's cumulant  $U_4$ , (c) the AF order parameter  $m_s$ , and (d) the susceptibility  $\chi_s$  for  $\alpha_{\text{LR}} = 0.5$ . The inset of (b) shows the crossing point of  $U_4$  used to locate the critical point  $\theta_c$ .

not fix the parity, an alternative quantity  $M_s(\mathbf{s}) = |\sum_i (-1)^i s_i|$  can characterize the order-disorder phase transition at the level of the RBM wave function. Thus, we consider the AF order parameter defined as

$$m_s = \frac{1}{L} \langle M_s \rangle_{\text{mc}}. \quad (8)$$

Near a critical point  $\theta_c$ , the order parameter measured in a finite system of size  $L$  is expected to behave asymptotically as  $m_s(\theta, L) \sim L^{-\beta/\nu} \mathcal{M}_o^{(\pm)}(|\theta - \theta_c|L^{1/\nu})$  with the critical exponents  $\beta$  and  $\nu$ , where  $\mathcal{M}_o^{(\pm)}$  is a size-independent scaling function. The corresponding susceptibility can be defined by the fluctuations of  $M_s$  as

$$\chi_s = \langle M_s^2 \rangle_{\text{mc}} - \langle M_s \rangle_{\text{mc}}^2, \quad (9)$$

which is also expected to follow the FSS ansatz of  $\chi_s(\theta, L) \sim L^{\gamma/\nu} \mathcal{X}_o((\theta - \theta_c)L^{1/\nu})$  associated with the exponent  $\gamma$ .

First we determine the critical point  $\theta_c$  for a given  $\alpha_{\text{LR}}$  by locating a crossing point of the fourth-order Binder's cumulant,

$$U_4 = 1 - \frac{\langle M_s^4 \rangle_{\text{mc}}}{3 \langle M_s^2 \rangle_{\text{mc}}^2}, \quad (10)$$

between the curves of different  $L$ 's. The FSS ansatz of the cumulant can be written as  $U_4(\theta, L) \sim \mathcal{U}_o((\theta - \theta_c)L^{1/\nu})$ . Although  $\mathcal{U}_o$  becomes independent of  $L$  for a large  $L$ , a finite-size correction can appear for small  $L$ 's. The leading-order finite-size correction is typically considered in a power-law form, which can be expressed as  $\theta_{L,2L}^* - \theta_c \propto L^{-\tilde{\omega}}$  for a crossing point  $\theta_{L,2L}^*$  identified between the two adjacent curves of sizes  $L$  and  $2L$ . We determine  $\theta_c$  based on this correction-to-scaling ansatz for the power-law extrapolation.

After locating the critical point  $\theta_c$ , we estimate the critical exponents  $\nu$ ,  $\beta$ , and  $\gamma$  by performing the standard FSS analysis with the FSS ansatz of  $m_s$ ,  $\chi_s$ , and  $U_4$  in the critical region. Figure 2 presents an example of the FSS analysis that we have done for  $\alpha_{\text{LR}} = 0.5$ , demonstrating that the data points

of different  $L$ 's fall well on a common scaling curve with our estimates of the critical exponents. The numerical estimates of the critical exponents and errors are measured using the pyfssa package [67, 68]. Our estimate of  $\theta_c$  and the critical exponents are listed in Table. I. Within the error bars, our estimates of the critical exponents are very close to the SR Ising values for all the values of  $\alpha_{\text{LR}}$  examined as shown in Fig. 2(a), which agrees well with the previous DMRG results [54, 55].

## B. Second Rényi entropy and central charge

The logarithmic system-size scaling of the entanglement entropy at a critical point in 1D is a useful universal property to measure the central charge of the CFT that characterizes the phase transition [69–71]. In the previous estimate of the central charge using the TDVP [52], DMRG [53], and generalized Hatree-Fork [58] methods, the von Neumann entanglement entropy was examined under the open boundary conditions (OBC). Here we investigate the second Rényi entropy measured using the RBM wave function under PBC. Considering the bipartition of a system into subsystems  $A$  and  $B$ , the Rényi

$\alpha_{\text{LR}}$	$\theta_c$	$\nu$	$\beta$	$\gamma$	$\eta$	$c_\infty$
3.0	0.8714(7)	1.00(4)	0.128(5)	1.77(5)	0.2510(4)	0.496(5)
2.5	0.9041(6)	1.01(2)	0.122(3)	1.76(5)	0.2491(2)	0.500(4)
2.0	0.9489(7)	1.00(2)	0.121(7)	1.76(7)	0.2518(7)	0.502(5)
1.5	1.012(1)	1.00(1)	0.126(9)	1.77(4)	0.2450(24)	0.508(4)
1.0	1.103(1)	1.01(3)	0.126(6)	1.78(7)	0.2398(35)	0.491(5)
0.5	1.251(1)	1.01(3)	0.127(5)	1.76(4)	0.2363(15)	0.454(8)

TABLE I. List of the critical points and exponents. The critical exponent  $\nu$ ,  $\beta$ , and  $\gamma$  are determined in the FSS analysis of the scaling curve collapse. The exponent  $\eta$  is estimated from the system-size scaling of the correlation function measured with a fixed  $r/L = 1/4$  at the critical point  $\theta_c$ . The central charge  $c_\infty$  is extracted from the logarithmic size scaling of the second Rényi entropy.

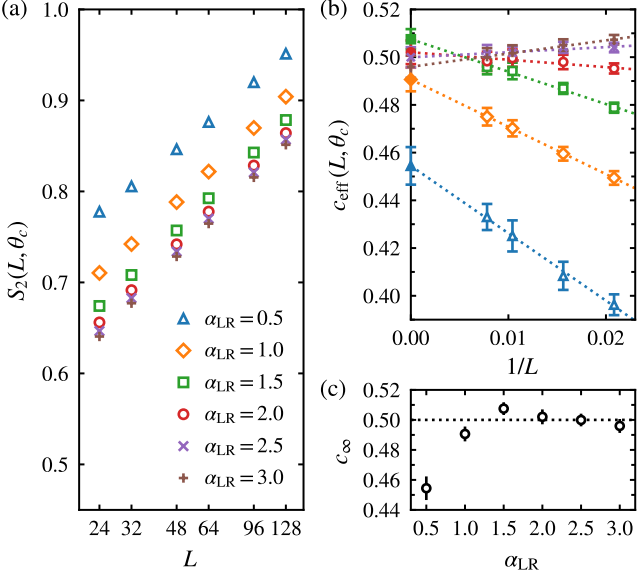


FIG. 3. Estimate of the central charge. (a) The second Rényi entropy  $S_2$  of a half chain is plotted at the critical point  $\theta_c$  as a function of system size  $L$ . (b) The effective central charge  $c_{\text{eff}}(L)$  is extrapolated to determine (c)  $c_{\infty}$  for the estimate of the central charge.

entanglement entropy of  $A$  at order  $n$  is written as

$$S_n(\rho_A) = \frac{1}{1-n} \ln \text{tr} \rho_A^n, \quad (11)$$

where  $\rho_A \equiv \text{tr}_B \rho$  is the reduced density matrix for a pure state  $\rho$ . The von Neumann entropy is recovered at the limit of  $n = 1$ . For the universality class fixed by the CFT, the von Neumann and Rényi entropies at the critical point indicate the same central charge  $c$  from the leading-order FSS behavior. For PBC, the asymptotic scaling behavior of  $S_n$  [71] can be written for the equal-size bipartition as

$$S_n = \frac{c}{6} \left( 1 + \frac{1}{n} \right) \ln L + c'_n, \quad (12)$$

where  $c'_n$  is a nonuniversal constant.

The second Rényi entropy  $S_2$  can be reliably measured in QMC calculations by using the replica trick [72], which has been successfully applied to the VMC calculations with the RBM wave function [13]. Here we only consider  $S_2$ , but a method was proposed to compute  $S_n$  of the higher  $n$  and to approximate  $S_1$  in a different NQS representation [73]. Measuring  $S_2$  requires two copies of the RBM state, namely  $\mathbf{s}^{(1)}$  and  $\mathbf{s}^{(2)}$ , sampled from the joint probability distribution  $P(\mathbf{s}^{(1)}, \mathbf{s}^{(2)}) \propto |\Psi(\mathbf{s}^{(1)})|^2 |\Psi(\mathbf{s}^{(2)})|^2$ . Each copy can be rewritten in a bipartite basis as  $\mathbf{s} \equiv (\mathbf{s}_A, \mathbf{s}_B)$ , where  $\mathbf{s}_A$  and  $\mathbf{s}_B$  are associated with the subsystems  $A$  and  $B$ . Then, one can obtain  $e^{-S_2}$  by measuring the swapping operator on  $A$  as

$$e^{-S_2} = \left\langle \frac{\Psi(\mathbf{s}_A^{(2)}, \mathbf{s}_B^{(1)})}{\Psi(\mathbf{s}_A^{(1)}, \mathbf{s}_B^{(1)})} \frac{\Psi(\mathbf{s}_A^{(1)}, \mathbf{s}_B^{(2)})}{\Psi(\mathbf{s}_A^{(2)}, \mathbf{s}_B^{(2)})} \right\rangle_{\text{mc}}. \quad (13)$$

We extract the central charge from the asymptotic behavior of  $S_2(L) = \frac{c}{4} \ln L + c'_2$ . From the measurements of  $S_2$  for two

system sizes  $L$  and  $L/2$ , the effective central charge for a finite  $L$  can be defined as

$$c_{\text{eff}}(L) = \frac{4}{\ln 2} [S_2(L) - S_2(L/2)], \quad (14)$$

which would reveal a finite-size correction for small  $L$ 's. The central charge is then formally written as  $c = c_{\infty} \equiv \lim_{L \rightarrow \infty} c_{\text{eff}}(L)$ , which can be evaluated by extrapolating  $c_{\text{eff}}(L)$  to infinite  $L$ . Figure 3 shows  $S_2(L)$  measured at the critical point in a finite system of size  $L$  and the corresponding finite-size behavior of  $c_{\text{eff}}(L)$ . We observe that  $c_{\text{eff}}(L)$  exhibits the power-law convergence behavior of  $|c_{\text{eff}}(L) - c_{\infty}| \propto 1/L$ . This behavior of  $c_{\text{eff}}(L)$  is consistent with the previous discussion on the finite-size correction of  $L^{-1/\nu}$  in the FSS analysis of the entanglement entropy [74].

Our estimate of  $c_{\infty}$  shows good agreement with  $c = 1/2$  of the SR Ising class for  $\alpha_{LR} \gtrsim 2$ . For  $\alpha_{LR} = 1.5$  and 1, the values of  $c_{\infty}$  are still close to 1/2 with the deviation of 0.01, although the systematic finite-size correction becomes stronger. For  $\alpha_{LR} = 0.5$ , the deviation from 1/2 is much larger than the error bar, implying the breakdown of the Ising universality and associated conformal symmetry. Our results are obtained from the second Rényi entropy under PBC, providing an interesting comparison to the previous results based on the von Neumann entropy under OBC [52, 53, 58]. All studies agree on a significant deviation from 1/2 for  $\alpha_{LR} < 1$ . However, we observe the tendency of  $c_{\infty}$  to decrease below 1/2, which is in contrast to the increase of  $c$  above 1/2 previously observed from the von Neumann entropy under OBC. Although we cannot rule out finite-size influences, the inconsistent trends of  $c$  found in the different measures of the entanglement with different boundary conditions may also be related to the breakdown of the conformal symmetry.

### C. Critical Binder ratio

Our RBM estimates of the critical exponents and the central charge given above agree with the previous TDVP and DMRG results, supporting the scenario that the conformal symmetry is broken at a sufficiently small  $\alpha_{LR}$ , while some of the critical exponents are still very close to the SR Ising values. However, it is still uncertain what the threshold value of  $\alpha_{LR}$  is below which the SR Ising universality class and its conformal invariance are broken. The numerical estimate of the central charge has given a significant deviation only for  $\alpha_{LR} < 1$ . The numerical deviation from 1/2 for a larger  $\alpha_{LR}$  is too weak to claim the breakdown of the SR Ising class while it shows strong finite corrections for  $\alpha_{LR} = 1$  and 1.5. Below we present an additional test for the breakdown of the SR Ising universality using the critical binder ratio that goes beyond the measure of critical exponents with the order parameter.

We examine the Binder ratio of the second and fourth moments of the staggered magnetization, which is written as  $Q \equiv \langle M_s^2 \rangle_{\text{mc}}^2 / \langle M_s^4 \rangle_{\text{mc}}$ . The Binder ratio at the critical point exhibits a particular value characterizing the universality, while the value depends on the boundary conditions and the aspect ratio of the system (see, for instance, Refs. [75, 76] and references therein). The universal ratio has been used as a reliable

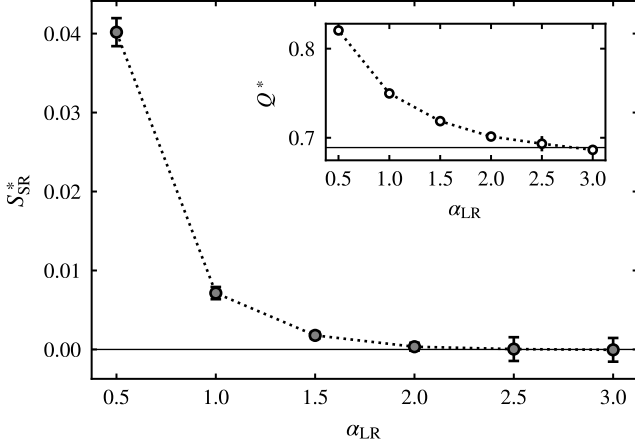


FIG. 4. Test of the universal Binder ratio. The self-combined ratio  $S_{SR}^*$  and the Binder ratio  $Q^*$  at the critical point are obtained in the power-law extrapolation to infinite size and plotted as a function of  $\alpha_{LR}$ . The horizontal solid lines indicate the SR limit.

ingredient to identify the universality class in the classical long-range Ising model [40], which inspires us to perform the same test for the universal ratio with the RBM wave function in AF-LR-TFIC

In the SR limit, we measure the value of  $Q_{SR}^* = 0.689(4)$  at the exact critical point  $\theta_c = \pi/4$  obtained in the power-law extrapolation to infinite size. While the ratio has not been known for the critical ground state of AF-TFIC in the SR limit, our estimate of  $Q_{SR}^*$ , which is equivalent to the cumulant  $U_4^* = 0.516(3)$ , agrees with the Monte Carlo estimate of  $U_4^* = 0.514(1)$  for the classical 2D Ising model subject to mixed boundary conditions where the system is periodic in one direction and open in the other direction [77].

Away from the SR limit, we consider the indicator called the self-combined binder ratio proposed in Ref. [40],

$$S_{SR}(L) = \frac{1}{Q_{SR}^*} Q(L) + \frac{1}{Q(L)} Q_{SR}^* - 2, \quad (15)$$

which is designed to remove the leading-order finite-size correction in  $Q(L)$  and exhibits better convergence in the extrapolation to infinite  $L$ . Figure 4 displays the value of  $S_{SR}^* \equiv \lim_{L \rightarrow \infty} S_{SR}(L)$  evaluated with finite-size data of  $Q(L)$  and then extrapolated to infinite  $L$ . It turns out that  $S_{SR}^*$  is almost zero for  $\alpha_{LR} = 3$  and 2.5. The deviation of  $S_{SR}^*$  appears for  $\alpha_{LR} \lesssim 2$  and increases as  $\alpha_{LR}$  decreases. The estimate of  $Q^* \equiv \lim_{L \rightarrow \infty} Q(L)$  shows a similar increase from the value of the SR limit as  $\alpha_{LR}$  decreases, although it still indicates a slight deviation even for  $\alpha_{LR} = 2.5$  and 3 where  $S_{SR}^*$  is zero. This is consistent with the observation in Ref. [40], indicating the better convergence of  $S_{SR}(L)$ . Our data suggest that the threshold of the SR Ising universality is possibly around  $\alpha_{LR} = 2$  above which  $S_{SR}^*$  remains zero within the error bars.

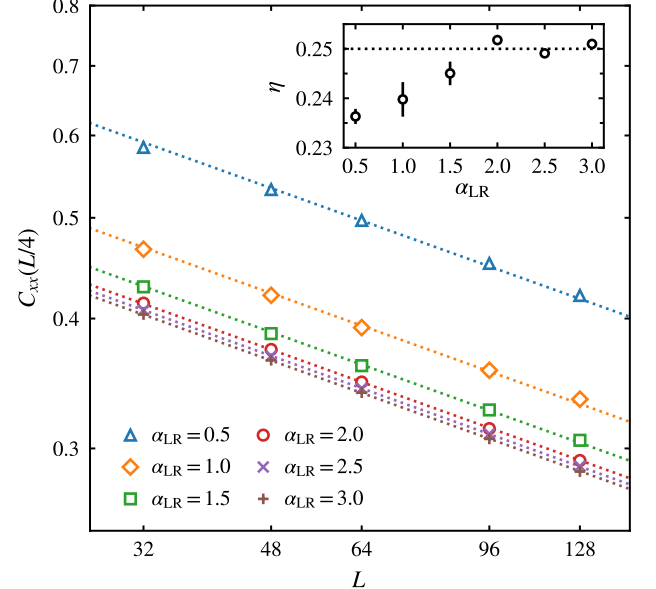


FIG. 5. Critical exponent of the spin-spin correlation function. The correlation function  $C_{xx}(r)$  at  $r = L/4$  is plotted as a function of the system size  $L$ . The inset shows the exponent  $\eta$  extracted from the data fitting to  $C_{xx}(L/4) \propto L^{-\eta}$ . The dotted lines are given for comparison with the SR Ising value  $\eta = 1/4$ .

#### D. CFT prediction of the correlation function

Our additional test for conformal invariance examines the correlation function to see if its shape agrees with the CFT description, following the strategy proposed in Ref. [62]. The PBC is imposed on our RBM wave function, which is essential to this test. We particularly consider the spin-spin correlation function defined as

$$C_{xx}(r) = \frac{1}{L-r} \sum_{i=1}^{L-r} \langle \hat{\sigma}_i^x \hat{\sigma}_{i+r}^x \rangle = \frac{1}{L-r} \sum_{i=1}^{L-r} \langle s_i s_{i+r} \rangle_{mc}, \quad (16)$$

where the distance  $r$  runs from 1 to  $L/2$  in the periodic chain, and the average over the sites is introduced for better statistics in the MC measurements.

The CFT in a cylindrical space-time geometry determines the asymptotic form of the two-point correlation function [78, 79]. In the SR limit, the 2D Ising universality and its CFT predicts that the correlation function in Eq. (16) behaves as

$$C_{xx}(r) \propto \left( \frac{1}{L \sin(\pi r/L)} \right)^{2\Delta_\sigma} \quad (17)$$

with the scaling dimension  $\Delta_\sigma = 1/8$ . A partial test of this prediction includes verification of the scaling dimension that is equivalent to the exponent  $\eta = 2\Delta_\sigma$  characterizing the algebraic decay of  $C_{xx}(r) \sim r^{-\eta}$  at a critical point. A more comprehensive test is to directly compare the form of the measured correlation function with the CFT-predicted form. While this strategy was originally proposed in the projector QMC simulations [62], we demonstrate below that it is also applicable to the RBM wave function.

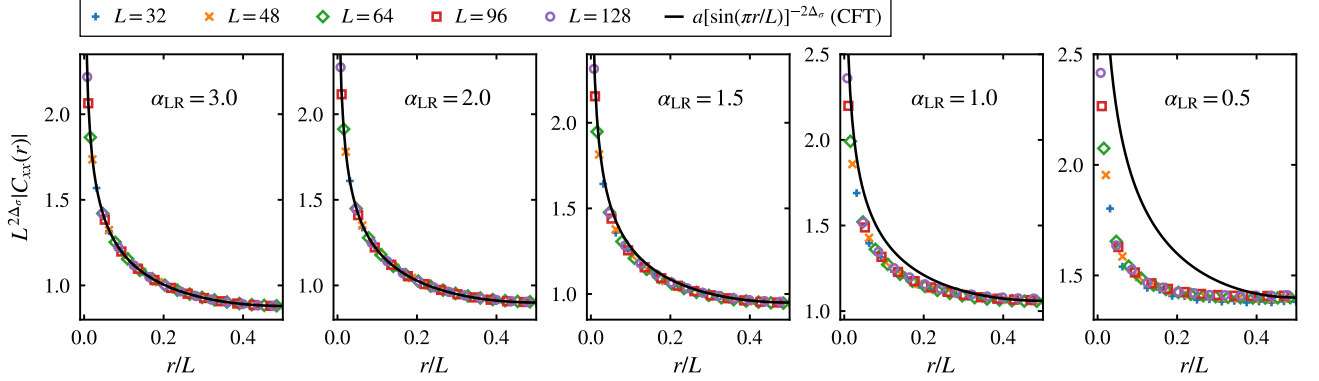


FIG. 6. FSS analysis of the spin-spin correlation function. The scaled data points of  $L^{2\Delta_\sigma} |C_{xx}(r)|$  for various  $L$ 's are examined as a function of  $r/L$  with the exponent  $2\Delta_\sigma$  being fixed at the SR Ising value  $1/4$ . The solid line indicates the predicted correlation function of the CFT  $a[\sin(\pi r/L)]^{-2\Delta_\sigma}$  given for comparison with the scaling curve of the measured correlation function.

We first measure the critical exponent  $\eta$  from the FSS behavior of  $C_{xx}(r)$  tested at a fixed  $r = L/4$  where  $C_{xx}$  is expected to decay as  $L^{-\eta}$ . As shown in Fig. 5, we obtain the estimate of  $\eta$  from the linear fit to the data points of  $C_{xx}(L/4)$  plotted as a function of  $L$  on the logarithmic scale. It turns out that our estimate of  $\eta$  decreases below  $1/4$  as  $\alpha_{LR}$  goes below 2. On the other hand, for  $\alpha_{LR} \geq 2$ , the estimate of  $\eta$  is consistent with the value of SR Ising  $1/4$ . These observations agree with the previous TDVP result [52].

The estimate of  $\eta$  suggests that the SR Ising class is not valid for  $\alpha_{LR} \lesssim 2$ . However, the deviation in  $\eta$  is very weak, which cannot be visually noticed, as the data is still well compared to the lines of  $L^{-1/4}$  given in Fig. 5. Additionally, assuming that the hyperscaling relation still holds,  $\eta < 1/4$  implies  $\gamma > 7/4$  and  $\beta < 1/8$  if  $\nu = 1$  is fixed. Such small changes in the exponents are hardly found in the analysis of the FSS collapse exemplified in Fig. 2. Within our limited numerical accuracy, it is difficult to precisely determine the universality class solely on the basis of the critical exponents.

For the direct test of the CFT-predicted form of the correlation function in Eq. (17), we perform the test for the FSS collapse of  $L^{2\Delta_\sigma} |C_{xx}(r)|$  shown in Fig. 6. We fix the exponent  $2\Delta_\sigma$  at the SR Ising value  $1/4$  for the test of the SR Ising class. Despite the fact that the measured value of  $\eta$  is not used, we still observe a good collapse of the data points falling on a common scaling curve at all  $\alpha_{LR}$  except with slight deviations found at  $\alpha_{LR} = 0.5$  where the measured value of  $\eta \approx 0.236$  is maximally different from  $1/4$ . In the graphical comparison between the observed scaling curve and the CFT prediction of  $L^{2\Delta_\sigma} |C_{xx}(r)| \propto [\sin(\pi r/L)]^{-2\Delta_\sigma}$ , we observe that the scaling curve starts to deviate from the CFT prediction at  $\alpha_{LR} \lesssim 2$ , and the deviation grows with a smaller  $\alpha_{LR}$ , which is consistent with the evidence found in our estimate of the critical Binder ratio presented above.

To have a closer view on the region of  $\alpha_{LR}$  where  $C_{xx}(r)$  starts to deviate from the CFT description, we consider the scaled correlation function proposed in Ref. [62], which is written as the ratio of the measured data of  $C_{xx}(r/L)$  and the

CFT description of Eq. (18),

$$C_{sc}(r/L) = \left[ L \sin\left(\pi \frac{r}{L}\right) \right]^{2\Delta_\sigma} |C_{xx}(r)|, \quad (18)$$

where  $2\Delta_\sigma$  is fixed at  $1/4$ . If the CFT of the 2D Ising universality class holds for this LR system, one can expect to see an asymptotically flat line of this scaled correlation function. Figure 7 displays  $C_{sc}(r/L)$  for  $\alpha_{LR}$  between 2 and 3. At  $\alpha_{LR} = 3$ , one can clearly see the flat solid line for  $L = 128$ . Although we have not shown here, our test in the SR limit has given the

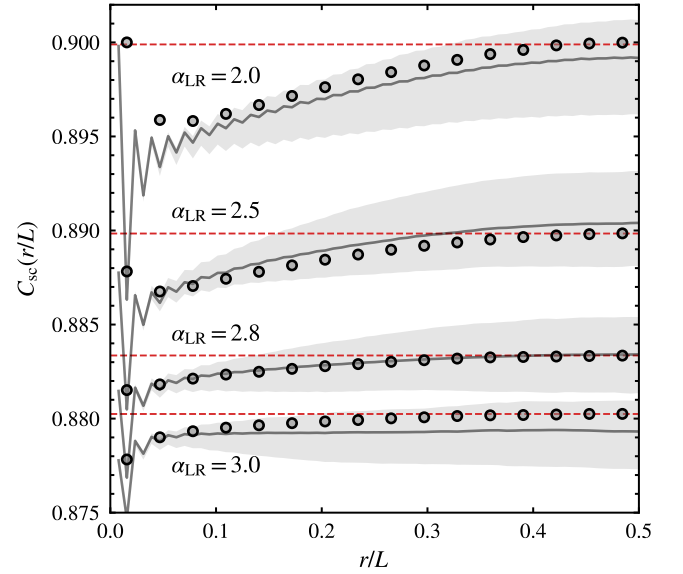


FIG. 7. Scaled correlation function for the test of the CFT description. Equation (18) is examined with ten samples of the RBM wave functions independently obtained in the VMC simulations at the critical point. The markers indicate the data of  $L = 64$  where the fluctuations over the RBM samples are smaller than the marker size. The gray solid line is the average over the samples for  $L = 128$ . The shade is filled between the minimum and maximum magnitudes of the data in the RBM wave function samples for  $L = 128$ .

same quality of the flat line displayed for  $\alpha_{LR} = 3$  within the fluctuations in the RBM samples.

It turns out that as we decrease  $\alpha_{LR}$ , the shape of  $C_{sc}(r/L)$  becomes more curved. As shown in Fig. 7, the range of  $r/L$  in the data points that correspond to the flat line tends to decrease as  $\alpha_{LR}$  decreases. Our observation indicates that a change in the shape of the correlation function gradually develops as  $\alpha_{LR}$  decreases below 3. However, it is difficult to detect a precise threshold value of  $\alpha_{LR}$  at which the asymptotic flat line would disappear, because the fluctuations in the RBM samples tend to increase with increasing system size. Our test of  $C_{sc}(r/L)$  suggests that the threshold for the SR Ising universality and the conformal invariance may be higher than  $\alpha_{LR} = 2$ , but it still needs much more precise calculations of the correlation function or more sensitive indicators.

#### IV. SUMMARY AND CONCLUSIONS

We have studied a quantum phase transition in the AF-LR-TFIC by using VMC methods based on the RBM trial wave function ansatz. Based on the FSS analysis to measure the critical exponents of the order parameter and extract the central charge from the second Rényi entropy, we have verified the previous TVDP and DMRG results [52–55], supporting the scenario [60] that the conformal symmetry is broken at a sufficiently small LR exponent  $\alpha_{LR}$  while some critical exponents are very close to the SR Ising values regardless of  $\alpha_{LR}$ . To identify the threshold for the breakdown of the SR Ising universality and the conformal symmetry, we have performed two additional tests that do not rely on the critical exponents. Our first test of the universal Binder ratio using its self-combined version [40] finds that the SR Ising value holds for  $\alpha_{LR} \gtrsim 2$  below which the ratio grows significantly as  $\alpha_{LR}$  decreases. In the other test for the validity of the CFT description of the spin-spin correlation function, our FSS analysis finds a visual difference between the measured scaling curve and the CFT prediction for  $\alpha_{LR} < 2$ . The detailed view given by the scaled

correlation function [62] indicates a gradual change that still occurs above  $\alpha_{LR} = 2$ , raising the possibility that the threshold may be at  $\alpha_{LR} \gtrsim 2$  while it should be less than 3 at which the measured data match well with the CFT description.

The measurement of the critical Binder ratio and the test of the CFT-predicted form of the correlation function reveal new evidence supporting the breakdown of the Ising universality and the conformal symmetry in the AF-LR-TFIC. However, despite our rough estimate on the threshold value of  $\alpha$  for the breakdown, the precise determination of the threshold still requires an intensive study to find sensitive indicators of conformal symmetry, such as Klein bottle entropy [80]. In addition, the apparent mismatch between the correlation function exponent and the other critical exponents needs to be reconciled to validate the hyperscaling relations in a future study with higher numerical accuracy.

Our VMC+RBM calculations for the FSS analysis of the criticality in this LR interacting system demonstrate the practical applicability of the NQS framework to the study of quantum phase transitions. While we have only considered a stoquastic Hamiltonian, the accuracy of the RBM wave function shown in our analysis of the critical ground state demonstrates its potential as an alternative or complementary tool to conventional zero-temperature methods.

#### ACKNOWLEDGMENTS

J.K. and D.K. contributed equally to this work. We thanks Synge Todo and Hong-Hao Tu for fruitful discussions in the ASG meeting at the PCS-IBS. This work was supported by the Basic Science Research Program through the National Research Foundation of Korea (NRF-2019R1F1A106321) and also by the KIAS associate member program. Computing resources are provided by the KISTI supercomputing center (KSC-2021-CRE-0165). We appreciate APCTP and PCS-IBS for its hospitality during the completion of this work.

---

[1] G. Carleo, I. Cirac, K. Cranmer, L. Daudet, M. Schuld, N. Tishby, L. Vogt-Maranto, and L. Zdeborová, Machine learning and the physical sciences, *Rev. Mod. Phys.* **91**, 045002 (2019).

[2] J. Carrasquilla, Machine learning for quantum matter, *Adv. Phys.* **5**, 179752 (2020).

[3] J. Carrasquilla and G. Torlai, How to use neural networks to investigate quantum many-body physics, *PRX Quantum* **2**, 040201 (2021).

[4] A. Dawid, J. Arnold, B. Requena, A. Gresch, M. Płodzień, K. Donatella, K. A. Nicoli, P. Stornati, R. Koch, M. Büttner, R. Okuła, G. Muñoz-Gil, R. A. Vargas-Hernández, A. Cervera-Lierta, J. Carrasquilla, V. Dunjko, M. Gabré, P. Huembeli, E. van Nieuwenburg, F. Vicentini, L. Wang, S. J. Wetzel, G. Carleo, E. Greplová, R. Krems, F. Marquardt, M. Tomza, M. Lewenstein, and A. Dauphin, Modern applications of machine learning in quantum sciences, *arXiv:2204.04198*.

[5] G. Carleo and M. Troyer, Solving the quantum many-body problem with artificial neural networks, *Science* **355**, 602 (2017).

[6] Y. Nomura, A. S. Darmawan, Y. Yamaji, and M. Imada, Restricted Boltzmann machine learning for solving strongly correlated quantum systems, *Phys. Rev. B* **96**, 205152 (2017).

[7] H. Saito, Solving the bose-hubbard model with machine learning, *J. Phys. Soc. Jpn.* **86**, 093001 (2017).

[8] M. Schmitt and M. Heyl, Quantum many-body dynamics in two dimensions with artificial neural networks, *Phys. Rev. Lett.* **125**, 100503 (2020).

[9] A. Nagy and V. Savona, Variational quantum monte carlo method with a neural-network ansatz for open quantum systems, *Phys. Rev. Lett.* **122**, 250501 (2019).

[10] M. J. Hartmann and G. Carleo, Neural-network approach to dissipative quantum many-body dynamics, *Phys. Rev. Lett.* **122**, 250502 (2019).

[11] F. Vicentini, A. Biella, N. Regnault, and C. Ciuti, Variational neural-network ansatz for steady states in open quantum systems, *Phys. Rev. Lett.* **122**, 250503 (2019).

[12] N. Yoshioka and R. Hamazaki, Constructing neural stationary states for open quantum many-body systems, *Phys. Rev. B* **99**, 214306 (2019).

[13] G. Torlai, G. Mazzola, J. Carrasquilla, M. Troyer, R. Melko, and G. Carleo, Neural-network quantum state tomography, *Nature Phys.* **14**, 447 (2018).

[14] G. Torlai, B. Timar, E. P. L. van Nieuwenburg, H. Levine, A. Omran, A. Keesling, H. Bernien, M. Greiner, V. Vuletić, M. D. Lukin, R. G. Melko, and M. Endres, Integrating neural networks with a quantum simulator for state reconstruction, *Phys. Rev. Lett.* **123**, 230504 (2019).

[15] Y. Nomura and M. Imada, Dirac-type nodal spin liquid revealed by refined quantum many-body solver using neural-network wave function, correlation ratio, and level spectroscopy, *Phys. Rev. X* **11**, 031034 (2021).

[16] A. Chen, K. Choo, N. Astrakhantsev, and T. Neupert, Neural network evolution strategy for solving quantum sign structures, *Phys. Rev. Res.* **4**, L022026 (2022).

[17] A. Szabó and C. Castelnovo, Neural network wave functions and the sign problem, *Phys. Rev. Res.* **2**, 033075 (2020).

[18] T. Westerhout, N. Astrakhantsev, K. S. Tikhonov, M. I. Katsnelson, and A. A. Bagrov, Generalization properties of neural network approximations to frustrated magnet ground states, *Nat. Commun.* **11**, 1593 (2020).

[19] F. Ferrari, F. Becca, and J. Carrasquilla, Neural gutzwiller-projected variational wave functions, *Phys. Rev. B* **100**, 125131 (2019).

[20] K. Choo, T. Neupert, and G. Carleo, Two-dimensional frustrated  $J_1-J_2$  model studied with neural network quantum states, *Phys. Rev. B* **100**, 125124 (2019).

[21] X. Liang, W.-Y. Liu, P.-Z. Lin, G.-C. Guo, Y.-S. Zhang, and L. He, Solving frustrated quantum many-particle models with convolutional neural networks, *Phys. Rev. B* **98**, 104426 (2018).

[22] K. Choo, A. Mezzacapo, and G. Carleo, Fermionic neural-network states for ab-initio electronic structure, *Nat. Commun.* **11**, 2368 (2020).

[23] D. Pfau, J. S. Spencer, A. G. D. G. Matthews, and W. M. C. Foulkes, Ab initio solution of the many-electron schrödinger equation with deep neural networks, *Phys. Rev. Res.* **2**, 033429 (2020).

[24] J. Hermann, Z. Schätzle, and F. Noé, Deep-neural-network solution of the electronic Schrödinger equation, *Nat. Chem.* **12**, 891 (2020).

[25] D.-L. Deng, X. Li, and S. Das Sarma, Quantum entanglement in neural network states, *Phys. Rev. X* **7**, 021021 (2017).

[26] J. Chen, S. Cheng, H. Xie, L. Wang, and T. Xiang, Equivalence of restricted Boltzmann machines and tensor network states, *Phys. Rev. B* **97**, 085104 (2018).

[27] I. Glasser, N. Pancotti, M. August, I. D. Rodriguez, and J. I. Cirac, Neural-network quantum states, string-bond states, and chiral topological states, *Phys. Rev. X* **8**, 011006 (2018).

[28] Y. Levine, O. Sharir, N. Cohen, and A. Shashua, Quantum entanglement in deep learning architectures, *Phys. Rev. Lett.* **122**, 065301 (2019).

[29] O. Sharir, A. Shashua, and G. Carleo, Neural tensor contractions and the expressive power of deep neural quantum states, *Phys. Rev. B* **106**, 205136 (2022).

[30] N. Defenu, T. Donner, T. Macrì, G. Pagano, S. Ruffo, and A. Trombettoni, Long-range interacting quantum systems, arXiv:2109.01063.

[31] C. Monroe, W. C. Campbell, L.-M. Duan, Z.-X. Gong, A. V. Gorshkov, P. W. Hess, R. Islam, K. Kim, N. M. Linke, G. Pagano, P. Richerme, C. Senko, and N. Y. Yao, Programmable quantum simulations of spin systems with trapped ions, *Rev. Mod. Phys.* **93**, 025001 (2021).

[32] R. Islam, E. E. Edwards, K. Kim, S. Korenblit, C. Noh, H. Carmichael, G.-D. Lin, L.-M. Duan, C.-C. Joseph Wang, J. K. Freericks, and C. Monroe, Onset of a quantum phase transition with a trapped ion quantum simulator, *Nat. Commun.* **2**, 377 (2011).

[33] J. Zhang, G. Pagano, P. W. Hess, A. Kyprianidis, P. Becker, H. Kaplan, A. V. Gorshkov, Z.-X. Gong, and C. Monroe, Observation of a many-body dynamical phase transition with a 53-qubit quantum simulator, *Nature* **551**, 601 (2017).

[34] B.-W. Li, Y.-K. Wu, Q.-X. Mei, R. Yao, W.-Q. Lian, M.-L. Cai, Y. Wang, B.-X. Qi, L. Yao, L. He, Z.-C. Zhou, and L.-M. Duan, Probing critical behavior of long-range transverse-field Ising model through quantum Kibble-Zurek mechanism, *PRX Quantum* **4**, 010302 (2023).

[35] S. Sachdev, *Quantum Phase Transitions*, 2nd ed. (Cambridge University Press, New York, 2011).

[36] N. Defenu, A. Codello, S. Ruffo, and A. Trombettoni, Criticality of spin systems with weak long-range interactions, *J. Phys. A: Math. Theor.* **53**, 143001 (2020).

[37] J. Sak, Recursion relations and fixed points for ferromagnets with long-range interactions, *Phys. Rev. B* **8**, 281 (1973).

[38] E. Luijten and H. W. J. Blöte, Boundary between long-range and short-range critical behavior in systems with algebraic interactions, *Phys. Rev. Lett.* **89**, 025703 (2002).

[39] M. C. Angelini, G. Parisi, and F. Ricci-Tersenghi, Relations between short-range and long-range ising models, *Phys. Rev. E* **89**, 062120 (2014).

[40] T. Horita, H. Suwa, and S. Todo, Upper and lower critical decay exponents of ising ferromagnets with long-range interaction, *Phys. Rev. E* **95**, 012143 (2017).

[41] C. Behan, L. Rastelli, S. Rychkov, and B. Zan, Long-range critical exponents near the short-range crossover, *Phys. Rev. Lett.* **118**, 241601 (2017).

[42] A. W. Sandvik, Ground states of a frustrated quantum spin chain with long-range interactions, *Phys. Rev. Lett.* **104**, 137204 (2010).

[43] S. Fey, S. C. Kapfer, and K. P. Schmidt, Quantum criticality of two-dimensional quantum magnets with long-range interactions, *Phys. Rev. Lett.* **122**, 017203 (2019).

[44] J. Koziol, S. Fey, S. C. Kapfer, and K. P. Schmidt, Quantum criticality of the transverse-field ising model with long-range interactions on triangular-lattice cylinders, *Phys. Rev. B* **100**, 144411 (2019).

[45] S. Huhmeniuk, Thermal Kosterlitz–Thouless transitions in the  $1/r^2$  long-range ferromagnetic quantum Ising chain revisited, *J. Stat. Mech.* **2020**, 063105.

[46] M. F. Paulos, S. Rychkov, B. C. van Rees, and B. Zan, Conformal invariance in the long-range Ising model, *Nuclear Physics B* **902**, 246 (2016).

[47] A. Dutta and J. K. Bhattacharjee, Phase transitions in the quantum Ising and rotor models with a long-range interaction, *Phys. Rev. B* **64**, 184106 (2001).

[48] M. Knap, A. Kantian, T. Giamarchi, I. Bloch, M. D. Lukin, and E. Demler, Probing real-space and time-resolved correlation functions with many-body ramsey interferometry, *Phys. Rev. Lett.* **111**, 147205 (2013).

[49] N. Defenu, A. Trombettoni, and S. Ruffo, Criticality and phase diagram of quantum long-range  $O(N)$  models, *Phys. Rev. B* **96**, 104432 (2017).

[50] Z. Zhu, G. Sun, W.-L. You, and D.-N. Shi, Fidelity and criticality of a quantum Ising chain with long-range interactions, *Phys. Rev. A* **98**, 023607 (2018).

[51] S. Shiratani and S. Todo, Stochastic approximation analy-

sis of dynamical quantum critical phenomena in long-range transverse-field Ising chain, arXiv:2305.14121.

[52] T. Koffel, M. Lewenstein, and L. Tagliacozzo, Entanglement entropy for the long-range Ising chain in a transverse field, *Phys. Rev. Lett.* **109**, 267203 (2012).

[53] D. Vodola, L. Lepori, E. Ercolessi, and G. Pupillo, Long-range Ising and Kitaev models: phases, correlations and edge modes, *New J. Phys.* **18**, 015001 (2016).

[54] G. Sun, Fidelity susceptibility study of quantum long-range antiferromagnetic Ising chain, *Phys. Rev. A* **96**, 043621 (2017).

[55] R. Puebla, O. Marty, and M. B. Plenio, Quantum Kibble-Zurek physics in long-range transverse-field Ising models, *Phys. Rev. A* **100**, 032115 (2019).

[56] S. Fey and K. P. Schmidt, Critical behavior of quantum magnets with long-range interactions in the thermodynamic limit, *Phys. Rev. B* **94**, 075156 (2016).

[57] J. A. Koziol, A. Langheld, S. C. Kapfer, and K. P. Schmidt, Quantum-critical properties of the long-range transverse-field Ising model from quantum Monte Carlo simulations, *Phys. Rev. B* **103**, 245135 (2021).

[58] M. P. Kaicher, D. Vodola, and S. B. Jäger, Mean-field treatment of the long-range transverse field Ising model with fermionic gaussian states, *Phys. Rev. B* **107**, 165144 (2023).

[59] D. Vodola, L. Lepori, E. Ercolessi, A. V. Gorshkov, and G. Pupillo, Kitaev chains with long-range pairing, *Phys. Rev. Lett.* **113**, 156402 (2014).

[60] L. Lepori, D. Vodola, G. Pupillo, G. Gori, and A. Trombettoni, Effective theory and breakdown of conformal symmetry in a long-range quantum chain, *Ann. Phys.* **374**, 35 (2016).

[61] T. Kuwahara and K. Saito, Area law of noncritical ground states in 1D long-range interacting systems, *Nat. Commun.* **11**, 4478 (2020).

[62] P. Patil, Y. Tang, E. Katz, and A. W. Sandvik, Indicators of conformal field theory: Entanglement entropy and multiple-point correlators, *Phys. Rev. B* **96**, 045140 (2017).

[63] C.-Y. Park and M. J. Kastoryano, Expressive power of complex-valued restricted Boltzmann machines for solving nonstoquastic Hamiltonians, *Phys. Rev. B* **106**, 134437 (2022).

[64] S. Sorella, Generalized Lanczos algorithm for variational quantum monte carlo, *Phys. Rev. B* **64**, 024512 (2001).

[65] S. Sorella, M. Casula, and D. Rocca, Weak binding between two aromatic rings: Feeling the van der Waals attraction by quantum Monte Carlo methods, *J. Chem. Phys.* **127**, 014105 (2007).

[66] E. Neuscamman, C. J. Umrigar, and G. K.-L. Chan, Optimizing large parameter sets in variational quantum monte carlo, *Phys. Rev. B* **85**, 045103 (2012).

[67] A. Sorge, pyfssa 0.7.6. zenodo (2015).

[68] O. Melchert, autoscale.py - a program for automatic finite-size scaling analyses: A user's guide, arXiv:0910.5403.

[69] G. Vidal, J. I. Latorre, E. Rico, and A. Kitaev, Entanglement in quantum critical phenomena, *Phys. Rev. Lett.* **90**, 227902 (2003).

[70] P. Calabrese and J. Cardy, Entanglement entropy and quantum field theory, *J. Stat. Mech.* **2004**, P06002.

[71] P. Calabrese and J. Cardy, Entanglement entropy and conformal field theory, *J. Phys. A: Math. Theor.* **42**, 504005 (2009).

[72] M. B. Hastings, I. González, A. B. Kallin, and R. G. Melko, Measuring Renyi entanglement entropy in quantum Monte Carlo simulations, *Phys. Rev. Lett.* **104**, 157201 (2010).

[73] Z. Wang and E. J. Davis, Calculating Rényi entropies with neural autoregressive quantum states, *Phys. Rev. A* **102**, 062413 (2020).

[74] M. Campostrini, A. Pelissetto, and E. Vicari, Finite-size scaling at quantum transitions, *Phys. Rev. B* **89**, 094516 (2014).

[75] V. Privman, *Finite Size Scaling and Numerical Simulation of Statistical Systems* (World Scientific, Singapore, 1990).

[76] W. Selke, The critical Binder cumulant for isotropic Ising models on square and triangular lattices, *J. Stat. Mech.* **2007**, P04008.

[77] W. Selke, Critical Binder cumulant of two-dimensional Ising models, *Eur. Phys. J. B* **51**, 223–228 (2006).

[78] M. Henkel, *Conformal Invariance and Critical Phenomena* (Springer-Verlag, Berlin Heidelberg, 1999).

[79] P. Francesco, P. Mathieu, and D. Sénéchal, *Conformal Field Theory* (Springer Science & Business Media, New York, 2012).

[80] H.-H. Tu, Universal entropy of conformal critical theories on a Klein bottle, *Phys. Rev. Lett.* **119**, 261603 (2017).